Available online at www.sciencedirect.com
ScienceDirect
Journal of Nuclear Materials 360 (2007) 104–117
journal of nuclear materials
www.elsevier.com/locate/jnucmat

Understanding of copper precipitation under electron or ion irradiations in FeCu0.1 wt% ferritic alloy by combination of experiments and modelling

B. Radiguet [a,*], A. Barbu [b], P. Pareige [a]

[a] Groupe de Physique des Matériaux UMR-CNRS 6634, Equipe de Recherche Technologique, no. 1000, Faculté des Sciences et Techniques, Site Universitaire du Madrillet, Avenue de l'Université B.P. 12, 76801 Saint Etienne du Rouvray, France
[b] Section de Recherches de Métallurgie Physique, Commissariat à l'Energie Atomique, Centre d'Etudes de Saclay, 91191 Gif-sur-Yvette cedex, France

Received 28 December 2005; accepted 11 September 2006

Abstract

This work is dedicated to the understanding of the basic processes involved in the formation of copper enriched clusters in low alloyed FeCu binary system (FeCu0.1 wt%) under irradiation at temperature close to 300 °C. Such an alloy was irradiated with electrons or with ions (Fe^+ or He^+) in order to deconvolute the effect of displacement cascades and the associated generation of point defect clusters (ion irradiations), and the super-saturation of mono-vacancies and self-interstitial atoms (electron irradiation). The microstructure of this alloy was characterised by tomographic atom probe. Experimental results were compared with results obtained with cluster dynamic model giving an estimation of the evolution of point defects (free or agglomerated) under irradiation on the one hand and describing homogeneous enhanced precipitation of copper on the other hand. The comparison between the results obtained on the different irradiation conditions and the model suggests that the point defect clusters (dislocation loops and/or nano-voids) created in displacement cascades play a major role in copper clustering in low copper alloy irradiated at 573 K.

PACS: 61.72.−y; 61.72.Bb; 61.82.Bg; 61.80.−x

1. Introduction

In a pressurised water reactor (PWR), the vessel – made of ferritic steel – is one of the most important barriers between the reactor core and the outside. Hardening and embrittlement of the vessel steel under neutron irradiation are one of the limitations of the lifetime of such reactors. It is well established that the degradation of the mechanical properties of vessel steel under irradiation is in relationship with the formation of a high number density ($>10^{23}$ m^{-3}) of very fine (~2 nm in diameter) solute clusters [1–12]. These clusters are enriched in one solute known to be in super-saturation [13,14] in iron at the temperature of irradiation (300 °C) – the copper – and also in some under saturated

* Corresponding author. Tel.: +33 2 32 95 51 40.
E-mail address: bertrand.radiguet@univ-rouen.fr (B. Radiguet).

0022-3115/$ - see front matter © 2006 Elsevier B.V. All rights reserved.
doi:10.1016/j.jnucmat.2006.09.007

solutes in iron [15]: manganese, nickel, silicon and phosphorus. At present time, if the homogeneous precipitation of copper is clearly the relevant mechanism in high copper alloys, the basic processes at the origin of the formation of these clusters in low copper alloys are still not well understood.

The main goal of this work is to bring information about the mechanism(s) that could explain the formation of solute clusters under irradiation. Three different possibilities are examined in this paper. First, some results suggest that solute clustering could occur directly inside displacement cascades, during the relaxation period [13,16]. Secondly, the super-saturation of mobile point defects accelerates the diffusion of the solutes atoms. Enhanced diffusion can result in enhanced homogeneous precipitation [17,18]. Finally, the third assumption examined here is heterogeneous precipitation on point defect clusters. Heterogeneous precipitation could be either due to the heterogeneous nucleation mechanism, or to radiation induced segregation [19–21].

To settle among the different hypothesis mentioned previously, specific irradiations are performed on a model alloy. For reasons of simplicity, the work presented in this paper is focused on the behaviour of copper. A FeCu0.1 wt% binary alloy is used for our experiments. This alloy has a relatively simple microstructure so the interpretation of the results is facilitated. It is irradiated with three kinds of incident particles. In the one hand, 3 MeV electrons are used. In this case, only isolated Frenkel pairs are created. The major effect of irradiation is then a super-saturation of free point defects resulting in enhanced diffusion of solute atoms and point defect fluxes. In the other hand, Fe^{+} (150 keV) and He^{+} (1 MeV) ions are used. Such irradiation results in the creation of displacement cascades (DC) during collisions between ions and target atoms. These cascades are known to result in the formation of a high number density of point defect clusters. Thus, comparing the different types of irradiation, it is possible to deconvolute the effect of the super-saturation of free point defects from the effect of displacement cascades and also from the effect of point defect clusters.

The evolution of the chemical microstructure during irradiation is followed by tomographic atom probe (TAP) which is one of the most efficient tool to observe and characterise nano-sized chemical features in metals [22–24]. In order to interpret the experimental results obtained with TAP, theoretical predictions obtained with the software 'Stopping and Ranging of Ions in Matter (SRIM 2003) [25] and the 'Cluster Dynamic for Precipitation and Vacancies and Interstitials Clustering' (CDPVIC) model described in [26] are used. This model mixes the 'Cluster Dynamic Vacancies and Interstitials Clustering' (CDVIC), which gives the evolution of the concentration of free point defects and point defects clusters under irradiation [27], and the 'Clusters Dynamic model for Precipitation' (CDP) which describes the homogeneous precipitation of one solute in a binary alloy [17]. The combination of these two models gives accurate prediction of homogeneous enhanced precipitation of copper under irradiation and an evaluation of the size and number density of point defect clusters, including the smallest ones witch are not visible with Transmission Electron Microscopy (TEM).

Our approach is then to compare the experimental number density and size of copper clusters with the calculated number densities of DC, point defect clusters and copper precipitates assuming homogeneous nucleation.

The first part of this paper describes the experimental procedure. Experimental results are presented in the second part. Finally, experimental results are discussed in the third part, tacking into account our calculations performed with the model.

2. Experimental procedure

2.1. Material

Results given in this paper concern FeCu0.1 wt% (0.088 at.%) binary alloy. Two different alloys were used in this work. The first was prepared by the Centre d'Etudes Nucléaires from Grenoble (CENG). It was cold rolled down to a thickness of 800 μm. Then it was subjected to recrystallization and homogenization treatment at 800 °C during 2 h under argon atmosphere, and after that, it was quenched under argon jet (~20 °C/s). This alloy was irradiated with electrons. The second alloy was made by the Centre d'Etudes de Chimie Métallurgique (CECM) at Vitry. After an austenitisation treatment (30 min at 1000 °C), it was maintained during 1 h at 850 °C followed by air quench (~10 °C/s). This alloy was used to perform ion irradiations. Each alloy, was made with high purity iron (C < 70 appm).

Atom probe experiments indicate that in each case a random solid solution is obtained. Indeed,

statistical χ^2 test are equal to 0.61 and 0.59 for the first and the second alloy respectively. The copper content of the ferritic matrix is 0.085 ± 0.007 at.% for the first alloy and 0.080 ± 0.006 at.% for the second. Optical micrography shows that the grain size is about one millimetre in diameter in each case Thus we are considering here that both alloys are identical.

2.2. Irradiation conditions

As mentioned before, three different types of irradiation were performed. In the first case, the alloy in the shape of a plate was irradiated with 3 MeV electrons in a Van de Graaff accelerator at the CENG. Only the centre of the plate is irradiated. Irradiated samples for atom probe experiments are cut from this part.

The two others kind of irradiations are Fe^+ and He^+ ion irradiations. In both cases, the already prepared atom probe samples were irradiated with an ion beam perpendicular to the axis of the tip. This procedure is due to the very small penetration depth of ions in the target (in particular for Fe^+ ions) which does not allow to irradiate bulk material and then cut atom probe samples.

Iron ion irradiations were performed in the Centre de Spectroscopie Nucléaire et de Spectrométrie de Masse (CSNSM) in Orsay, France. Fe^+ ions were used to create the primary knocked atoms (PKA) that will generate displacement cascades with energy between few hundred eV and about 145 keV. Under this condition, the primary damage is not homogeneous in the material. As it will be shown later, the dose rate strongly depends of the distance from the surface. In order to have the maximum primary damage in the analysed volume of the TAP samples, the chosen energy of Fe^+ ions was 150 keV.

Helium ion irradiations were performed in a Van de Graaff accelerator in Commissariat à l'Energie Atomique (CEA) in Saclay, France. He^+ ions with an energy equal to 1 MeV were used. Such ions go right through the TAP sample, thus no helium is implanted. As described later, the main advantage of using this kind of ions is that the production rate of point defects is similar to those obtained with 150 keV Fe^+ ions, but helium ions creates 10 times less large displacement cascades ($E_{PKA} \geqslant 10$ keV) than Fe^+ ions.

For each type of irradiation, the detailed conditions are reported in Table 1. As it can be observed in this table, electrons produce a dose rate comparable to the dose rate received by a PWR vessel, whereas the dose rate due to ion irradiations (in dpa NRT [28]) is largely higher. Concerning iron ion irradiations, four different fluences were used corresponding to 17, 100, 840 and 2500 seconds of irradiation. Irradiation temperature, the usual operation temperature of the vessel of water-pressurised reactor, was 300 °C.

These irradiation conditions were chosen in order to compare electron and ion irradiations, dividing effects of displacement cascades, super-saturation of free point defects and influence of point defects clusters.

2.3. Atom probe experiment

All the experiments were performed with tomographic atom probe (TAP). They were carried out using a pulse fraction of 19% and a temperature of 50 K in order to prevent preferential evaporation of copper [29]. In every case a low evaporation flux, about 0.03 detected ions per pulse, was maintained in order to minimise the risk of rupture of the tip during analysis and also in order to prevent pile up effect [30].

After each atom probe experiment, the data were always treated on the same way. First algorithm to identify clusters was applied to volume. This tool allows to identify small clusters which are not visible 'with eyes' in the 3D-reconstruction. The principle is

Table 1
Irradiation conditions for electron and ion irradiations

	T (K)	Flux ($m^{-2}\,s^{-1}$)	Fluence (m^{-2})	Dose rate (dpa NRT s^{-1})	Dose (dpa NRT)
Electrons	563	9.4×10^{17}	5×10^{24}	5.6×10^{-9}	3×10^{-3}
Fe ions	573	5×10^{14}	$8.5 \times 10^{15} \rightarrow 1.2 \times 10^{18}$	1.4×10^{-4}	$2.4 \times 10^{-3} \rightarrow 0.35$
He ions	573	2.6×10^{17}	6.5×10^{20}	2.6×10^{-5}	0.065

Four different times of irradiation were used for iron ion irradiations (17, 100, 840 and 2500 s) corresponding to fluences between 8.5×10^{15} and 1.2×10^{18} m^{-2}. Concerning ion irradiations, dose and dose rate are reported in dpa NRT.

the following. A sphere with a fixed radius (0.8 nm was chosen because it contains 100 detected atoms with an atomic volume equals to 0.0117 nm^3 and a detection efficiency equals to 0.5) is placed on each atom. If the concentration of copper inside this sphere is higher than a fixed concentration threshold (set to 4 at.%) the atom is considered to be in a cluster. This method and the chosen parameters allow detection of copper clusters containing at least five copper detected atoms. If solute clusters are identified, they are characterised in term of size (radius or number of detected copper atoms), chemical composition and number density. The matrix composition is then the composition of the all volume without clusters. If any cluster is identified, the matrix composition is assimilated to the composition of the analysed volume. In this case, statistical χ^2 test of the spatial distribution of solute atoms is done, in order to determine if copper is still homogeneously distributed after irradiation.

3. Experimental results

3.1. Electron irradiation

The position of copper atoms in a small volume analysed with TAP after electron irradiation is represented in Fig. 1. As it is clearly revealed, and confirmed by computed statistic analyses of the data set, no copper clusters (containing at least five detected copper atoms) are observed under this electron irradiation condition.

The χ^2 test indicates that the spatial distribution of copper atoms is not significantly different from a binomial distribution (χ^2 test = 0.73). After electron irradiation, under this condition, copper atoms are still randomly distributed in the ferritic matrix. The copper content of the matrix is still close to those measured in the reference material: 0.084 ± 0.005 at.%.

Thus electron irradiation has no detectable influence on copper atoms distribution. We could also mentioned that taking into account the whole analysed volume, if copper clusters are formed under this irradiation condition, their number density is smaller than 4×10^{22} m^{-3}.

3.2. Fe^+ ion irradiation

The second kind of irradiation is iron ion irradiations at four fluences. The first one corresponds to only 17 s. The results obtained after 17 s of irradiation are the following:

- No copper cluster is detected (Fig. 2).
- A binomial like distribution of copper atoms is observed (χ^2 test = 0.88).
- The copper content of the matrix is close to the nominal composition (0.10 ± 0.01 at.%).

Here again, this irradiation condition has no detectable influence on the spatial distribution of copper atoms. The total analysed volume in this case is 15 000 nm^3. So if copper clusters are formed, there number density is less than 7×10^{22} m^{-3}.

The examination of the second condition of irradiation with iron ions (corresponding to 100 s) shows different results. A slight evolution of the distribution of copper atoms is detected and the copper concentration in the matrix is: 0.082 ± 0.005 at.%.

These observations are consistent with the presence of a number density equal to 8×10^{22} m^{-3} of copper clusters as shown in Fig. 3. One of the clusters depicted in Fig. 3 is a diffuse atmosphere containing only six detected copper atoms ('detected' means that the number of copper atoms inside clusters are not corrected, taking into account the detection efficiency of TAP, ~50%). The second one is a pure copper precipitate (96 ± 4 at.% of copper). Its

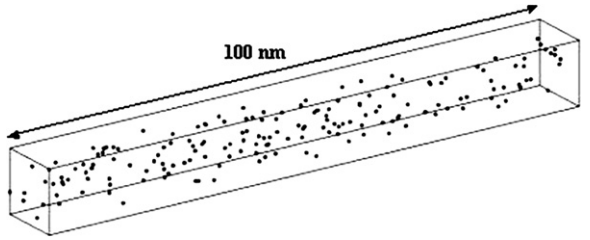

Fig. 1. Atom map of the copper atoms after electron irradiations. Only copper atoms are represented. No copper cluster is observed.

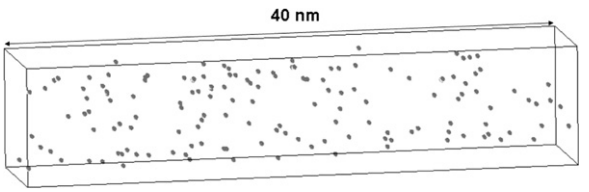

Fig. 2. Atom map of the copper atoms after iron ion irradiations during 17 s. No copper cluster is observed. In this volume, the distribution of copper atoms is binomial like.

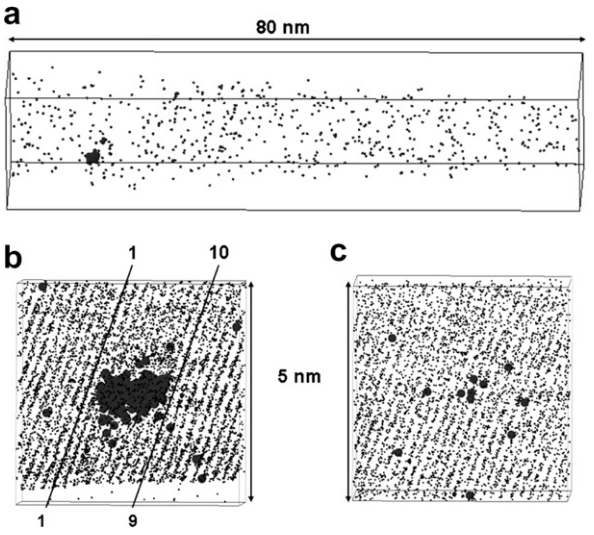

Fig. 3. (a) Three-dimensional reconstruction of a small volume analysed after 100 s of irradiation with iron ions. Only copper atoms are represented. (b) A pure copper precipitate and (c) a very small diffuse copper cluster are observed in this volume. On the two zooms, copper atoms are grey circles and iron atoms are black points. (1 1 0) planes in the ferritic matrix are visible. The number of planes above the copper precipitate is higher than below, showing that copper precipitate is on a edge dislocation line ($b = a/2$ (1 1 0)).

radius is close to 1 nm. As it can be observed in Fig. 3(b) where (1 1 0) planes of the ferritic matrix are also represented, this precipitate is located in the core region of the edge component of an edge dislocation line ($b = a/2\ \langle 1\,1\,0\rangle$).

The third fluence corresponds to 840 s. After irradiation, the copper content of the matrix drops to (0.055 ± 0.005) at.%. This lack of copper in the matrix is due to the presence of a large amount of small copper enriched clusters as shown in Fig. 4.

The number density of copper clusters is $10^{24}\ m^{-3}$. Their size is around 2 nm in diameter. The mean value of detected copper atoms in these clusters is 20. However, it varies from 5 for the smallest up to 70 copper atoms for the biggest. Their copper content varies from 20 at.% up to 70 at.% with a mean value equal to (42 ± 2) at.%. These clusters are not well-defined precipitates but diffuse objects.

The last fluence is obtained after 2500 s. The copper content in the matrix is then 0.045 ± 0.004 at.%. Here again a large number density ($5.5 \times 10^{23}\ m^{-3}$) of copper enriched clusters is detected. As observed in Fig. 5, these clusters are very different from ones to the others. Indeed, some clusters contain only few copper atoms (as observed after 100 s irradiation) whereas some others are large copper precipitates with a diameter up to 4 nm. The mean value of detected copper atoms in this population of clusters is 80. This value varies from 5 for the smallest up to 540 copper atoms for the biggest. Their copper content varies from 5 at.% up to 80 at.%. The mean concentration is (38 ± 3) at.%.

All the results obtained on iron ion irradiations are summarised in Table 2. Concerning the matrix composition, the copper concentration decreases with fluence. The diminution of copper in the matrix is faster during the first 840 s than during the following 1660 s. Nucleation of copper clusters occurs since 100 s of irradiation. Then, when the fluence increases, their mean size (number of copper atoms and radius) increases. Their number density also increases, at least during the first 840 s. Moreover, even after 2500 s, there are still very small clusters containing only few copper atoms (as observed after 100 s). Thus, it seems that the clusters nucleated at the beginning of the irradiation grow with fluence and at the same time nucleation of new clusters occurs continuously during all irradiation time. However, the number density of copper clusters is lower after 2500 s than after 840 s. Two phenomena could explain this observation. First, considering the size of the volume analysed with TAP, the difference between the number densities measured after 840 and 2500 s could be too low to be statisti-

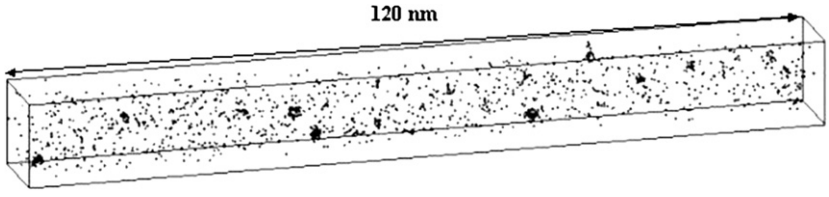

Fig. 4. Microstructure of the alloy after 840 s of iron ion irradiation. Only copper atoms are represented. A high number density of copper enriched clusters is observed.

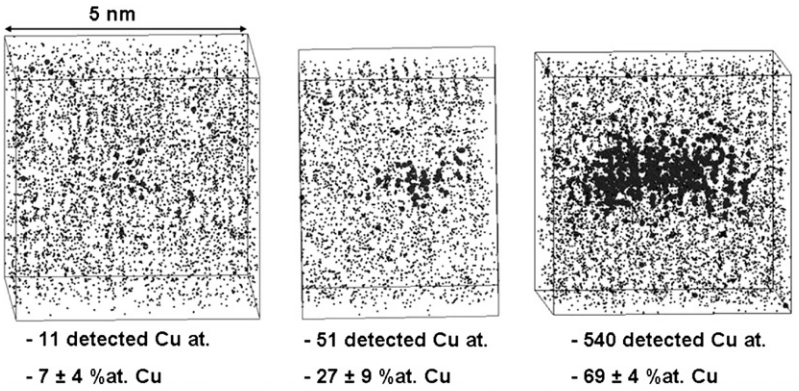

Fig. 5. Zoom on different copper enriched clusters observed after iron ion irradiation during 2500 s. Circles are copper atoms and points are iron atoms.

Table 2
Summary of the different results observed after iron ion irradiations

	Matrix at.% of Cu	Copper enriched clusters		
		Number density (m^{-3})	Size (in Cu atoms)	at.% of Cu
Fe 17s	0.10 ± 0.01	$<7 \times 10^{22}$	–	–
Fe 100s	0.082 ± 0.005	4×10^{22}	6 (6)	–
Fe 840 s	0.055 ± 0.005	1×10^{24}	22 (5–70)	42 ± 2 (20–70)
Fe 2500s	0.045 ± 0.004	5.5×10^{23}	81 (5–540)	38 ± 3 (5–80)

Values concerning copper enriched clusters are mean values. Between parenthesis are given minimum and maximum values.

cally significant. Second, it is possible that there is a coarsening of the clusters.

3.3. He^+ ion irradiation

After irradiation with helium ions during 2500 s, the matrix contains only (0.046 ± 0.008) at.% of copper. As it can be seen in Fig. 6, the microstructure obtained after helium ion irradiations is very similar to those observed after iron ion irradiations during 840 s.

Indeed, a high number density (8×10^{23} m^{-3}) of small copper enriched clusters is observed. These clusters measure 1.2 nm in radius. They contain around 30 detected copper atoms and their copper level is equal to (25 ± 5) at.%.

4. Modelling and discussion

Experimental results show that copper clustering only occurs after ion (He^+ and Fe^+) irradiations, if irradiation time is long enough ($\geqslant 100$ s). In order to interpret these results and determine the process at the origin of copper clustering, the CDPVIC model was used. It is described in the next section.

4.1. Cluster dynamic model

The so called Cluster Dynamics model used here is an advance modelling based on rate theory considering the evolution of point defect cluster distributions and precipitates under irradiation. The system is considered as a gas of clusters, possibly

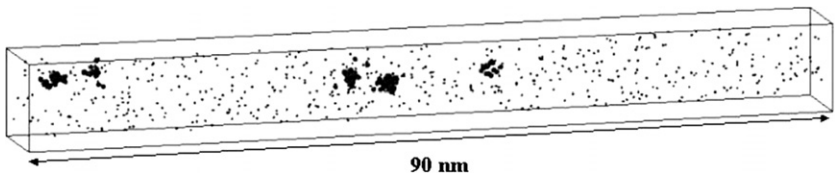

Fig. 6. Atom map of the copper atoms after helium ion irradiation during 2500 s. A high number density of copper enriched clusters is observed.

mobile up to a given size. The CD code used in our calculations (CDPVIC) is fully described in [26]. It combines the CDVIC code, which is described in [27], and the CDP model that is presented in [17,31]. The CDVIC code gives the evolution of the population of point defects and point defect clusters under irradiation. Point defect and point defect clusters are produced at a certain rate depending on the irradiation flux. Considering the complexity of the mechanism concerning SIA clusters (three possible different configurations), the absence of precise knowledge about the reaction between SIA clusters and about the effect of impurity on SIA clusters mobility, a simplified model is considered in the code (only one type of interstitial clusters and no mobility for interstitial clusters but for single SIA). SIA's and vacancies can interact with clusters giving larger or smaller clusters. They can also disappear on fixed sink as dislocations, grain boundaries or surfaces. The CDP code considers the homogeneous precipitation of a dilute solute, here copper. Merging the two allows to calculate enhanced homogeneous precipitation of copper under irradiation, considering the effect of vacancy super-saturation. Indeed, the copper diffusivity under irradiation, D^*_{Cu} is assumed to be equal to

$$D^*_{Cu} = D^{th}_{Cu} \cdot \frac{C^*_V}{C^{th}_V}, \quad (1)$$

where D^{th}_{Cu} is the thermal diffusivity of copper atoms, C^*_V is the vacancy concentration under irradiation and C^{th}_V is the equilibrium vacancy concentration at the temperature of irradiation. The parameters introduced in the model are reported in Table 3.

Concerning the copper precipitation, the parameters are the solubility limit, C_{eq} and the thermal copper diffusivity, D^{th}_{Cu}. The thermal copper diffusivity is given by

$$D^{th}_{Cu} = D_0 \cdot \exp\left(-\frac{Q}{k \cdot T}\right), \quad (2)$$

where Q is the activation energy, D_0 the pre-exponential factor, k the Boltzman constant and T the temperature in Kelvin. The parameters used in our calculations are the same than in Ref. [26] (see Table 3). The solubility limit is given by

$$C_{eq} = \exp\left(\frac{\Delta S}{k}\right) \cdot \exp\left(-\frac{\Omega}{k \cdot T}\right), \quad (3)$$

where ΔS is a non-configurational entropy term and Ω is the demixing energy. The values used in our calculations (Table 3) are those given by Miloudi [13] on the base of experimental results obtained with a FeCu binary alloy annealed between 450 and 550 °C. It is worth noticing that copper solubility calculated with these values at 290 °C ($C_{eq} = 5 \times 10^{-3}$ at.%) is closed to those given by [26] at the same temperature ($C_{eq} = 4 \times 10^{-3}$ at.%).

Table 3
Parameters used in the model

	Electron	Ion
Grain size or thickness of the thin foil	1 mm	80 nm
Dislocation density	10^8 cm^{-2}	
Vacancy formation energy	1.6 eV	
SIA formation energy	4.3 eV	
Vacancy migration energy	1.3 eV	
SIA migration energy	0.3 eV	
Pre-exponential factor of vacancy diffusivity	1 cm^2 s^{-1}	
Pre-exponential factor of SIA diffusivity	4×10^{-4} cm^2 s^{-1}	
Recombination radius	6.5 A	
Capture efficiency of vacancies by dislocations	1.0	
Capture efficiency of SIA by dislocations	1.2	
Di-vacancy binding energy	0.2 eV	
Di-interstitial binding energy	1.2 eV	
Non-configurational entropy ($\Delta S/k$)	0.056	
Mixing energy (Ω/k)	5560 K^{-1}	
Pre-exponential factor of Cu diffusivity	0.627 cm^2 s^{-1}	
Cu migration activation energy	2.288 eV	

Excepted for grain size or thickness of the thin foil and solubility limit of copper, parameters are the same than in Refs. [26,27].

Concerning point defects, the parameters are the same than in [27]. They were determined on the base of experimental results obtained on FeCu0.1 wt% in situ electron irradiated in a high voltage electron microscope.

Another important parameter is either the grain size in the case of a bulk material or the 'thickness' of the tip. These values determine the sink strength of grain boundaries in the first case and the sink strength of surfaces in the second case. Concerning electron irradiation, the samples are plate shaped, with a thickness of 800 μm. In this case, we consider bulk material with grain size equals to 1 mm. During ion irradiation, the already prepared atom probe samples were irradiated. Considering the size of a tip (40–100 nm in diameter) it is clear that the effect of surface is preponderant compared to the effect of grain boundaries on the elimination of mobile point defects. However, only the strength of surfaces of a thin foil can be taken into account in the model. Monte Carlo calculations performed by Domain [32] show that there is no significant difference between the evolution of point defects created by

displacement cascades with energy equal to 20 keV in a tip (cylinder of 20 nm in diameter) or a thin foil with the same thickness. So the tip was assimilated to a thin foil in our calculations.

All the point defect clusters are assumed to be immobile but single SIA's and vacancies. This choice is based on Ref. [33] where it is shown that the microstructural changes of electron irradiated model ferritic alloys can be fitted with more realistic parameters assuming that the point defect clusters are not mobile.

Finally, in order to use this model with a high realistic description, the knowledge of point defects and point defect clusters production rates is needed.

In the case of electron irradiations, the calculation of the primary damage is relatively simple. Indeed, in this case there is no displacement cascade. Only Frenkel pairs are created. The dose rate in term of displacement per atom per second (dpa s^{-1}) is given by this expression: dpa $s^{-1} = \sigma_d \cdot \Phi_e$ where σ_d is the displacement cross section and ϕ_e is the electron flux (9.4×10^{17} m^{-2} s^{-1} for this experiment). Using the table of Oen [34], with an average displacement threshold of 40 eV for iron [35], a dose rate of 5.6×10^{-9} dpa s^{-1} and dose equals to 3×10^{-3} dpa are obtained.

As far as ion irradiation is concerned, the calculation of primary damage is more complex due to the presence of displacement cascades. Indeed, the production rate has to be estimated not only for monomers but also for point defect clusters directly created inside displacement cascades. Thus, we have to estimate not only the number of dpa s^{-1} but also the proportion of point defects in point defect clusters. In order to do this, SRIM calculation [25] and molecular dynamic results [36] were combined to introduce a primary damage as realistic as possible in the CDPVIC model.

First, SRIM calculations with Fe^+ (150 keV) or He^+ (1 MeV) ions are performed. Among the different results given by SRIM, the energy transmitted to target atom by incident ion during each collision is used. For each collision, the depth of the impact is known. For example, the energy given by iron ions during each collision with atoms versus depth is reported in Fig. 7. These data set is cut in intervals of energy and depth and the number of PKA in each interval ($N_{PKA}^{E,p}$) is determined. Thus the number of PKA per atom per second for each energy interval and for each depth ($N_{PKA}^{E,p}$/s/at) is calculated with this expression:

$$N_{PKA}^{E,p}/s/at = \frac{N_{PKA}^{E,p} \cdot \Phi}{N_{ion} \cdot N_{at} \cdot \Delta p}, \quad (4)$$

where ϕ is the ion flux, N_{ion} is the number of incident ions used during SRIM calculation, Δp is the size of the interval of depth and N_{at} is the number of target atoms contained in a volume of 1 $m^2 \times \Delta p$.

Thus, for each depth, the energy distribution of PKA is known. As it can be seen in Fig. 7, PKA with energy higher than 20 keV exist. Now, it is shown by molecular dynamic that PKA with energy higher than 20 keV, generate well separated sub-cas-

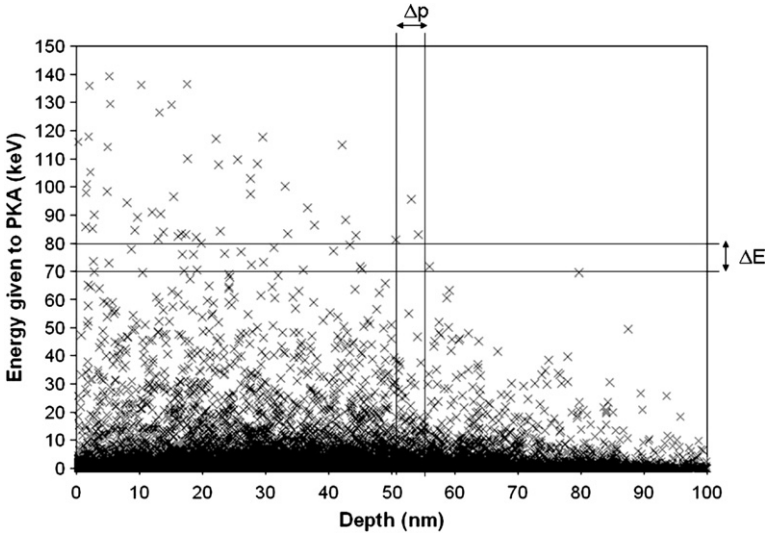

Fig. 7. Energy given by Fe^+ incident ions during each collision with Fe target atoms (SRIM calculation with 500 incident ions).

cades similar to single cascades that would be obtained at lower energy [37].

In order to be as realistic as possible, for PKA with energy higher than 20 keV, new SRIM calculations are performed. The previous procedure is then applied to the SRIM results obtained for these PKA. These PKA are then replaced in the original distribution (for Fe^+ ions of 150 keV or He^+ ions of 1 MeV) by their distribution obtained with SRIM. Thus, for each depth, the energy distribution of sub-cascades is known. In the case of iron ion irradiations, this distribution strongly depends of the depth whereas helium ion irradiations create an homogeneous damage through the sample. Fig. 8 represents such a distribution for both kinds of ions. Concerning iron irradiations, it is the distribution calculated at a depth corresponding to the volume analysed in a TAP sample. It is worth noticing that iron ions create 10 times more sub-cascades with energy higher than 10 keV than helium ions. Indeed, the number of sub-cascades with an energy higher than 10 keV that occur in the material is equal to $5\times10^{22}\,m^{-3}\,s^{-1}$ during Fe^+ irradiations, and $4\times10^{21}\,m^{-3}\,s^{-1}$ during He^+ irradiations.

The primary damage due to displacement cascades of these different energies is given by molecular dynamic. Using the molecular dynamic results given in Ref. [36] and the sub-cascades distribution calculated previously, it is possible to estimate the primary damage. The dose rate (in dpa s^{-1}) received

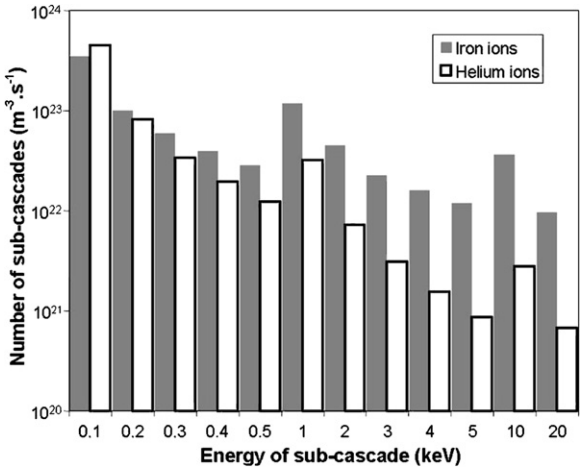

Fig. 8. Sub-cascade spectra calculated with the method described in Section 2.1. The spectrum due to iron ion irradiations is in grey and those due to helium ion irradiations is in white. Iron ions produce 10 times more sub-cascades with 'high' energy ($\geqslant$10 keV) than helium ions.

Table 4
Production rate of point defects in terms of displacement per atom for electron and ion irradiations

	dpa s^{-1}	dpa
Electron	5.6×10^{-9}	3×10^{-3}
Fe^+ ion	4×10^{-5}	$6.8\times10^{-4}\rightarrow0.1$
He^+ ion	1.2×10^{-5}	3×10^{-2}

During electron irradiations all the point defects are created in the form of monomers. Fe^+ irradiations create 50% of vacancies and 70% of interstitials in the form of monomers. He^+ irradiations create more than 80% of the point defects in the form of monomers.

by the part of the sample which is analysed during TAP experiments is equal to 4×10^{-5} dpa s^{-1} during iron ion irradiations, and 10^{-5} dpa s^{-1} during helium ion irradiations. These values are smaller than those given by the NRT model. Irradiation conditions in term of dpa introduced in the model are reported in Table 4 both for electron and ion irradiations.

During ion irradiations, only a part of these production rates results in the formation of mono-vacancies or mono-interstitials. The proportion of monomers and point defects clusters created directly is represented in Fig. 9. According to our calculation of the primary damage, only 50% of the vacancies and 70% of the interstitials are created on the form of monomers during Fe^+ irradiations. During He^+ irradiations, more than 80% of the point defects are created on the form of monomers. This difference between the two kinds of ions is due to the fact that iron ions produce more displacement cascades than helium ions. The point defects that are not free are inside clusters containing up to 29 vacancies or 12 interstitials. These results were used as source terms in the model.

4.2. Discussion

Each hypothesis presented in the introduction is now examined using the results obtained with calculation, in order to determine if it can explain the formation of copper clusters observed after ion (Fe^+ and He^+) irradiations and the absence of such clusters after electron irradiation.

4.2.1. Effect of displacement cascades

In order to determine if the observed copper clusters are formed inside DC, the number of DC with energy higher than 10 keV produced in a volume

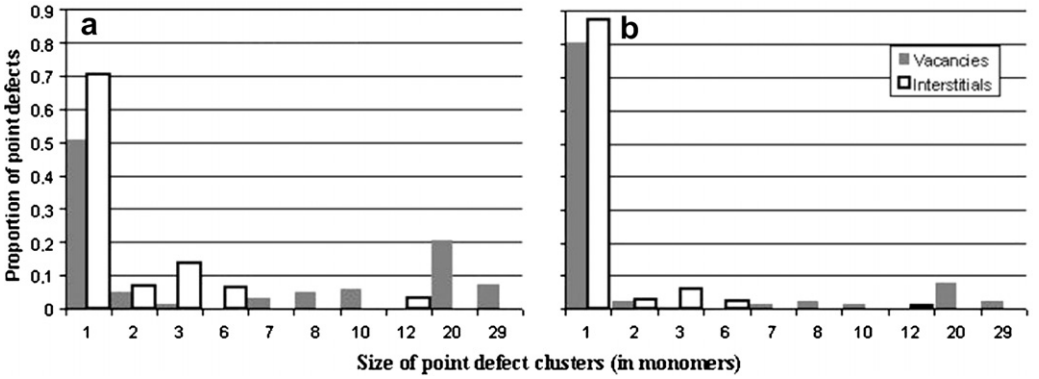

Fig. 9. Repartition of the point defects created each second during (a) iron and (b) helium ion irradiations between the different point defect clusters. Vacancy clusters surviving at the end of displacement cascades are larger than interstitial clusters.

analysed by TAP is compared with the number of copper clusters observed in the same volume.

We are interested in the number of DC with energy equal or higher than 10 keV because only such cascades have a sufficient volume. Indeed, the volume affected by a cascade between 10 and 20 keV is a sphere with a diameter equal to 3–5 nm [36]. Tacking into account the level of copper in the alloy (0.09 at.%), such spheres contain between 10 and 30 copper atoms. The detection efficiency of TAP is close to 50%. Thus, if copper clustering occurs directly in DC, small copper clusters (containing 5–15 detected copper atoms) can be observed with TAP after ion irradiations. DC with lower energy affect a too small volume to allow gathering of enough copper atoms to be detected by TAP (inside cascades with energy lower than 10 keV, less than 5 copper atoms can gather).

Using SRIM, it was shown that iron ion irradiations produce $5\times10^{22}\,m^{-3}\,s^{-1}$ DC ($E \geqslant 10$ keV). After Fe^{+} irradiations during 17 and 100 s, the whole volume investigated with TAP is $1.5\times10^{-23}\,m^{3}$ and $2.4\times10^{-23}\,m^{3}$ respectively. Thus the number of DC occurred in these volumes is equal to 135. Now, no copper cluster was observed after 17 s and only two was detected after 100 s. Thus, if DC are at the origin of copper clustering, this process has a very low efficiency (less than 1 copper cluster for 60 DC).

According to the calculations, He^{+} irradiations produce 10 times less DC than iron ions ($4\times10^{21}\,m^{-3}\,s^{-1}$). The whole volume analysed with TAP after helium irradiation is 6000 nm^3. In this volume about 60 DC occurred during irradiation. Tacking into account the efficiency of DC estimated previously, at the most one copper cluster should be detected in this volume, if copper clusters are formed inside DC. Now five clusters were detected by TAP in this volume. This observation suggests that the observed copper clusters after helium ion irradiations are not formed inside DC.

4.2.2. Homogeneous precipitation

Fig. 10 shows the evolution of the atomic fraction of vacancies and SIA during helium and iron ions irradiations. For both kinds of ions, the same behaviour is observed. The concentration of free point defects quickly reaches a maximum and starts to decrease after only few seconds because the samples are very small and mobile point defects reach the surface very quickly. During these ion irradiations, a steady state is not reached. However, excepted during the beginning of irradiation, the evolution of free point defect concentration is low. The concentrations of vacancies and SIA are close to 10^{-7} and 10^{-12} respectively, during the major part of irradiation for both kind of incident particles (Fe^{+} and He^{+}).

As it was said before, assuming a vacancy mechanism for copper diffusion, the copper diffusivity can be written $D^{*}_{Cu} = D^{th}_{Cu}\cdot\frac{C^{*}_{V}}{C^{th}_{V}}$. Taking into account the vacancy concentration under irradiation calculated previously ($\sim10^{-7}$) and the equilibrium vacancies concentration at 300 °C ($\sim3\times10^{-14}$), the copper diffusivity under irradiation is about 10^{7} times more than the thermal diffusivity. Is such a high diffusivity of copper atoms able to produce a high number density of copper clusters by enhanced homogeneous precipitation? The results given by the model about homogeneous copper precipitation indicate that some small (1–2 nm in diameter) copper precipitates are formed during ion irradiation.

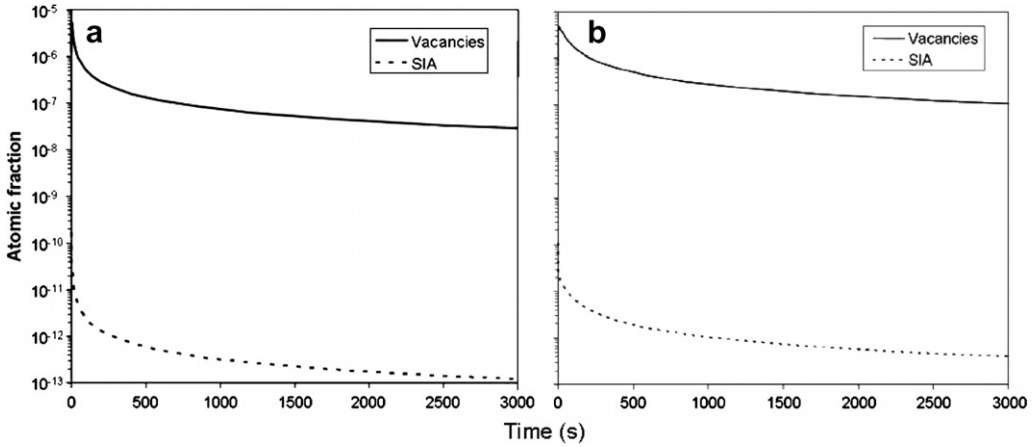

Fig. 10. Evolution of the atomic fraction of mono-vacancies and SIA during (a) iron ion and (b) helium ion irradiations, calculated with the model. Black and dotted lines represent the evolutions of mono-vacancies and SIA, respectively.

However, the estimated number density of precipitate due to homogeneous enhanced precipitation is extremely low (1.1×10^{16} m^{-3}). Features with a so low number density are not observable with atom probe. Indeed a typical volume analysed with this technique is $20 \times 20 \times 100$ nm^3. To have a chance to observe one feature during an analyse, its number density has to be higher than 10^{23} m^{-3}. Moreover, a so low number density of so small precipitates has no influence about the calculated composition of the matrix. So, no evolution of the matrix composition is expected at the end of the irradiation. Thus, according to the model, there is no chance to observe copper cluster formed by homogeneous enhanced precipitation during ion irradiations with TAP. So it can be concluded that the copper cluster observed after ion irradiations are not formed by this mechanism.

In order to get more information about homogeneous precipitation, it's of interest to compare ion and electron irradiations. The evolution of the concentration of free point defects during electron irradiation is reported in Fig. 11. SIA, which are the fastest point defects, annihilate on sinks since the first second of irradiation and their concentration decreases. As long as vacancies have not reached sinks, their concentration increases. After 7500 s, vacancies also annihilate on sinks and a steady state is established. Compared to the total irradiation time (5×10^5 s), the steady state is quickly reached. The atomic fraction of monomers is then 2×10^{-7} for vacancies and 5×10^{-13} for interstitials. It is worth noticing that these concentrations are very similar to those calculated for ion irradiations.

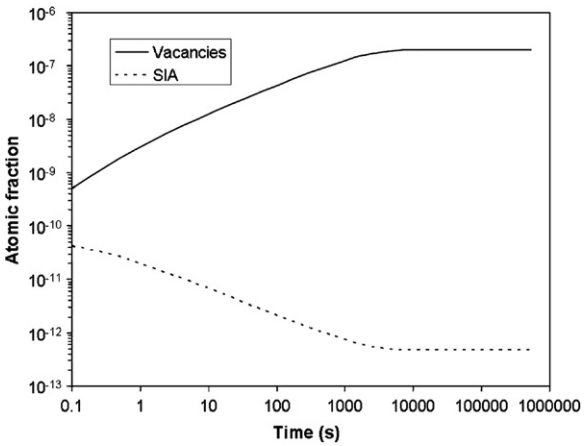

Fig. 11. Evolution of the atomic fraction of mono vacancies and SIA during electron irradiation.

So copper diffusivity is practically the same during both kinds of irradiations (ions and electrons). Now, after electron irradiations, no copper cluster was observed with TAP. Thus, this experiment clearly shows that even with high super-saturation of mobile point defects during long time, copper homogeneous enhanced precipitation is not observed at temperature close to 300 °C in low -copper alloys (<0.1 at.%). This result agrees well with those given by the model. Indeed, according to it, under electron irradiations, copper enhanced homogeneous precipitation occurs but results in a very low number density (5×10^{16} m^{-3}) of big copper precipitates (about 60 nm in diameter). Taking into account their number density, there is no chance to observe these precipitates with TAP and even with

TEM as well. Moreover, the copper content of the matrix at the end of irradiation calculated with the model is equal to 0.075 at.%. This value is very close to the measured concentration in the irradiated material.

Finally, the comparison between electron and ion irradiations indicate that homogeneous enhanced precipitation of copper is not able to explain the high number density of copper clusters observed after irradiations with iron or helium ions. Moreover, the model indicates that in our conditions of irradiation, homogeneous precipitation of copper produce only a extremely low number density of clusters. Thus another mechanism should be involved to describe copper clustering during ion irradiations.

4.2.3. Heterogeneous precipitation

Since DC and homogeneous enhanced precipitation seems to be not able to explain the formation of the high number density of copper clusters observed after ion irradiations, a third process is now examined: heterogeneous precipitation on point defect clusters. In order to determine if this process can play a role in copper clustering under irradiation, another result given by the model is used: the number density of point defect clusters as a function of their size at the end of the different kinds of irradiations (Figs. 12 and 13).

The size distribution of vacancies and interstitials clusters at the end of electron irradiations ($\sim 5 \times 10^5$ s) estimated with the model is reported in Fig. 12. The binding energy of interstitials is higher than those of vacancies (see Table 3) so the number density of interstitial clusters (dislocation loops) is higher than those of vacancy clusters (nano-void). It is maximal for loops containing about 600 interstitials ($\sim$7 nm in diameter). However, the main point is that the number density of both kinds of point defect clusters is still very low at the end of electron irradiations. Indeed, the number density of point defect clusters containing more than 10 monomers is equal to 4×10^{18} m^{-3} for interstitial clusters and 2×10^{13} m^{-3} for vacancy

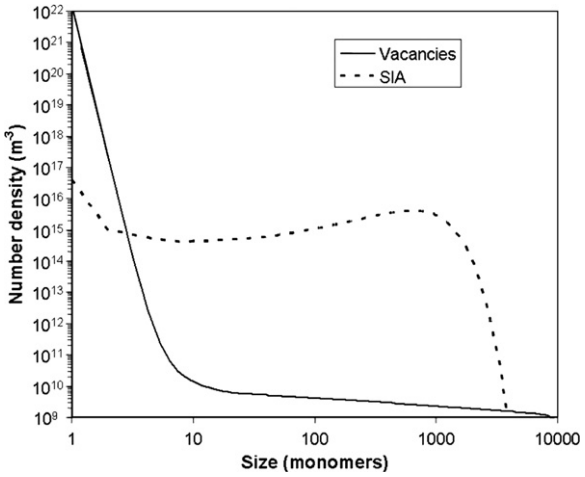

Fig. 12. Distribution of point defect clusters at the end of electron irradiation. Number density of vacancy (solid line) and SIA (dotted line) clusters is represented as a function of cluster size.

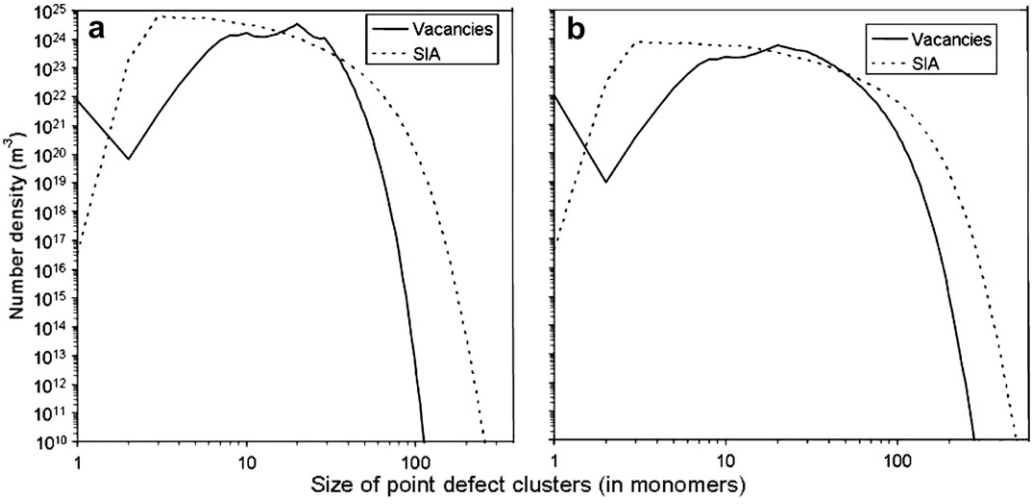

Fig. 13. Distribution of point defect clusters (a) after 840 s of iron ion irradiation and (b) 2500 s of helium ion irradiation. Number density of vacancy (solid line) and SIA (dotted line) clusters is represented as a function of cluster size.

clusters. Taking into account the typical size of a volume analysed with TAP ($20 \times 20 \times 100\ nm^3$), it appears clearly that if copper clusters are formed by heterogeneous precipitation on point defect clusters during electron irradiations, there is no chance to detect them with this technique.

Concerning ion irradiations, the results given by the model are dramatically different. The differences appear in Fig. 13. It represents the size distribution of point defect clusters after 840 s of Fe^+ irradiations and 2500 s of He^+ irradiations (that is to say the same fluence for both kind of ions in term of dpa: 0.03 dpa). Whereas electron irradiation results in the formation of a very low density of point defect clusters, ion irradiations create a very high number density of such clusters. After helium ion irradiations during 2500 s the material contains $1.2 \times 10^{25}\ m^{-3}$ interstitial loops and $1.4 \times 10^{25}\ m^{-3}$ nano-voids. The calculated number density of point defect clusters at the end of the different irradiations with iron ions (17–2500 s) varies from 7×10^{23} to $9 \times 10^{25}\ m^{-3}$ for interstitial clusters and from 8.7×10^{23} to $10^{26}\ m^{-3}$ for vacancy clusters. The difference between electron and ion irradiations is due to the creation mode of point defects. In the case of ion irradiations, lot of small point defect clusters are nucleated inside displacement cascades.

Another difference between electron and ion irradiation is the size of the point defect clusters. Whereas these clusters contain hundreds SIA or vacancies after electron irradiation, they are smaller in the case of ion irradiation. Indeed, as it can be observed in Fig. 13, vacancy and interstitial clusters contain less than 50 monomers, a value corresponding to a size smaller than 2 and 1 nm for interstitial and vacancy cluster respectively. Considering the time of irradiation, in the case of ions (2500 s at maximum), the point defect clusters have not enough time to grow.

The comparison between experimental results (copper clusters) and calculations (point defect clusters) after ion irradiations shows that the material contains always more point defect clusters than copper clusters. Thus there is always enough point defect clusters in order that each copper cluster is located on a point defect cluster. Taking into account this observation and the previous conclusions about the effects of DC and homogeneous precipitation, it appears that heterogeneous precipitation of copper on small point defect clusters is the only way to explain the formation of copper clusters observed after ion irradiations. This mechanism also explain why no copper cluster was detected after electron irradiations (in this case the number density of point defect clusters is too low to induce any detectable copper precipitation on interstitial or vacancy clusters with TAP).

5. Conclusion

To determine what are be basic processes at the origin of the formation of copper enriched clusters in low copper ferritic alloys irradiated at temperature close to 300 °C, specific irradiations with electrons or ions on FeCu0.1 wt% binary alloy were performed. A cluster dynamic model giving an estimation of the evolution of the population of point defects and predicting homogeneous enhanced precipitation of copper was used to interpret the experimental results obtained with TAP. The major results are the following:

(1) Iron ion irradiations during short time (17 and 100 s) compared with helium ion irradiations suggest that the nucleation of copper clusters does not occur inside displacement cascades.
(2) Electron irradiation show that, even with a very high super-saturation of mono-vacancies ($\sim 10^7$ times more than equilibrium concentration), homogeneous enhanced precipitation of copper does not occur in a significant way in low copper alloy at 300 °C. This observation is in good agreement with the model that predicts a very low number density of copper precipitates in this case. The fact that copper homogeneous precipitation is certainly not at the origin of the formation of the copper enriched clusters observed after ion irradiation is also supported by the model.
(3) The comparison between electron and ion irradiations reveals the major role of point defects clusters in the nucleation of copper clusters. Indeed, with the same estimated diffusivity of copper atoms, the formation of copper clusters occurs only when the model predicts a high number density of point defect clusters. Thus it appears that under ion irradiations at 300 °C in low copper content alloy, the copper clusters are very likely formed by heterogeneous precipitation on PD clusters. DC play an important role in this process because they are at the origin of the formation of point defects clusters.

(4) Finally, Fe^{+} irradiations at four different times have shown that when fluence increases, there is a growth of copper clusters and maybe a phenomenon of coarsening.

Acknowledgements

The authors gratefully acknowledge the organisers of CPR SMIRN for their support. Many thanks to C. Domain from EDF research centre for fruitful discussions. The authors also thank M.O. Ruault, S. Gautrot and O Kaitasov from the CSNSM and Y. Serruys from CEA for the realisation of ion irradiations.

References

[1] C.A. English, W.J. Phythian, J.T. Buswell, J.R. Hawthorn, P.H.N. Ray, in: Effects of Radiations on Materials: 15th International Symposium, ASTM STP, 1125; R.E. Stoller, A.S. Kumar, D.S. Gelles (Eds.), ASTM, Philadelphia, vol. 93, 1992.
[2] M.K. Miller, M.G. Burke, J. Nucl. Mater. 195 (1992) 68.
[3] P. Pareige, M.K. Millller, Appl. Surf. Sci. 94&95 (1996) 370.
[4] G.R. Odette, C.L. Liu, B.D. Wirth, Mater. Res. Soc., Proc. B 7 (1996).
[5] P. Pareige, R.E. Stoller, K.F. Russel, M.K. Miller, J. Nucl. Mater. 249 (1997) 165.
[6] P. Auger, P. Pareige, S. Welzel, J-C. Van Duysen, J. Nucl. Mater. 280 (2000) 331.
[7] Y. Nagai, Z. Tang, M. Hassegawa, T. Kanai, M. Saneyasu, Phys. Rev. B 63 (2001).
[8] R.G. Carter, N. Soneda, K. Dohi, J.M. Hyde, C.A. English, W.L. Server, J. Nucl. Mater. 298 (2001) 211.
[9] M.K. Miller, K.F. Russel, M.A. Sokolov, R.K. Nanstad, J. Nucl. Mater. 320 (2003) 177.
[10] K. Fukuya, K. Ohno, H. Nakata, S. Dumbill, J.M. Hyde, J. Nucl. Mater. 312 (2003) 163.
[11] P. Pareige, B. Radiguet, A. Suvorov, M. Kozodaev, E. Krasicov, O. Zabusov, J.P. Massoud, Surf. Interf. Anal. 36 (2004) 581.
[12] M.K. Miller, M.A. Sokolov, R.K. Nanstad, K.F. Russel, J. Nucl. Mater. 351 (2006) 216.
[13] S. Miloudi, Thèse de doctorat, Université de Paris XI Orsay, 1997.
[14] M.K. Miller, K.F. Russel, P. Pareige, M.J. Starink, R.C. Thomson, Mater. Sci. Eng. A 520 (1998) 49.
[15] Binary Alloy Phase Diagram, American Society for Metals, 1986.
[16] P. Pareige, F. Pérocheau, P. Auger, S. Jumel, H. Bernas, Nucl. Instrum. and Meth. B 178 (2001) 233.
[17] M.H. Mathon, A. Barbu, F. Dunstetter, F. Maury, N. Laurenzelli, C.H. de Novion, J. Nucl. Mater. 245 (1997) 224.
[18] G.R. Odette, G.E. Lucas, Radiat. Eff. Def. Solids 144 (1998) 189.
[19] G. Martin, R. Cauvin, A. Barbu, in: F. Dolfi (Ed.), Transformations During Irradiation, 1983, p. 47.
[20] H. Wiedersich, N.Q. Lam, in: F. Dolfi (Ed.),Transformations During Irradiation, 1983, p. 1.
[21] S. Ishino, Y. Chimi Bagiyono, T. Tobita, N. Ishikawa, M. Suzuki, A. Iwabase, J. Nucl. Mater. 323 (2003) 354.
[22] D. Blavette, A. Bostel, A. Menand, J. Trace Microprobe Techn. 12 (1&2) (1994) 17.
[23] A. Menand, E. Cadel, C. Pareige, D. Blavette, Ultramicroscopy 78 (1999) 63.
[24] D. Blavette, A. Bostel, J.M. Sarrau, B. Deconihout, A. Menand, Nature 363 (1993) 432.
[25] J.F. Ziegler, Nucl. Instrum. and Meth. B 219&220 (2004) 1027.
[26] F. Christien, A. Barbu, J. Nucl. Mater. 324 (2004) 90.
[27] A. Hardouin Duparc, C. Moingeon, N. Smetniansky-de-Grande, A. Barbu, J. Nucl. Mater. 302 (2002) 1143.
[28] M.J. Norgett, M.T. Robinson, I.M. Torrens, Nucl. Eng. Des. 33 (1975) 50.
[29] P. Pareige, Thèse de Doctorat, Université de Rouen, 1994.
[30] M.K. Miller, G.D.W. Smith, Atom Probe Microanalysis: Principles and Applications to Materials Problems, Material Research Society, 1989, p. 177.
[31] E. Clouet, A. Barbu, L. Lae, G. Martin, Acta Metall. 53 (2005) 2313.
[32] C. Domain, private communication.
[33] A. Barbu, Oral communication, IGRDM 11, 2003.
[34] O.S. Oen, Oak Ridge, 1973.
[35] ASTM E521, Standard practise for neutron radiation damage simulation by charged-particle irradiation, Annual Book of ASTM Standards, vol. 12.02, American Society of Testing and Materials, West Conshohocken, PA, 1996.
[36] C. Domain, J. Ruste, C. Becquart, Rapport (EDF), 1998.
[37] R.E. Stoller, G.R. Odette, B.D. Wirth, J. Nucl. Mater. 251 (1997) 49.